JOURNAL OF CATALYSIS 143, 215–226 (1993)

Selective Oxidation of Butane to Maleic Anhydride on a Vanadium–Phosphorus Oxide Catalyst: Promotional Effects of Zirconium

RAVINDRA SANT[1] AND ARVIND VARMA

Department of Chemical Engineering, University of Notre Dame, Notre Dame, Indiana 46556

Received November 2, 1992; revised March 19, 1993

This study examines the role of zirconium as a promoter in the selective oxidation of *n*-butane to maleic anhydride on a vanadium–phosphorus oxide catalyst. Reaction studies show that low levels of zirconium (Zr/V = 0.03) *decrease* the temperature of maximum yield relative to the unpromoted catalyst. Higher levels of zirconium (Zr/V = 0.13) result in lower yields. $^{16}O_2$–$^{18}O_2$ exchange measurements show no evidence for oxygen exchange between the gas phase and the bulk lattice at 400°C, in agreement with other studies. X-ray diffraction (XRD) and X-ray photoelectron spectroscopy (XPS) measurements are combined with the reaction studies to indicate a probable structural role for zirconium as a promoter.

INTRODUCTION

The selective catalytic oxidation of *n*-butane to maleic anhydride is a reaction of significant commercial importance. The catalyst consists primarily of vanadium-phosphorus oxides (VPO), although a variety of promoter elements are added in the industrial context. Catalysts are prepared in either aqueous or organic media. In the aqueous route, a reducing agent such as hydrochloric acid is usually added to the aqueous vanadium solution, and the phosphorus source (e.g., phosphoric acid) is then introduced in order to precipitate the vanadium–phosphorus oxide. In the organic route, an organic solvent is used for dissolving the vanadium salt, and this or another organic solvent is used as the reducing agent. The phosphorus source is also kept free of water. The organic route is of more recent origin and has been shown to yield catalysts with higher surface areas (*1*). The catalyst-reaction system has been studied extensively, and summaries of these studies are available in various reviews (*2, 3*). Whereas most studies in the open literature have focused on the reaction pathways, and the structure and utilization of the *un*promoted catalyst, there have been relatively few studies of promotional effects. Promoted catalysts have been the subject of numerous patents, but little is known regarding their function and mode of action. Hutchings (*1*) has reviewed the literature concerning the use of promoters in VPO catalysts.

Cobalt, zirconium, zinc, and molybdenum are among the promoter elements whose effects have been examined in some detail. Hodnett and Delmon (*4*) studied the influence of cobalt on the βVPO_5 phase (P/V = 1, Co/V = 0–0.05; all elemental ratios are mole or atomic ratios unless stated otherwise) and proposed that Co acted in two ways: at lower levels (Co/V up to 0.015), the influence on solid-state properties increased the selectivity, while at higher levels, the formation of CO and CO_2 was promoted by excess Co on the surface. Ai (*5*) used different methods to prepare ZrO_2-containing VPO catalysts. The catalyst with the highest activity and selectivity was prepared by

[1] Present address: Cabot Corporation, Technology Division, P.O. Box 5001, Pampa, TX 79066.

0021-9517/93 $5.00

mixing the VPO catalyst precursor powder with two solutions of ethylene glycol, one containing $ZrOCl_2$ and the other H_3PO_4. The original VPO precursor had P/V = 1.1 and was prepared by the organic route; the final catalyst had P/V = 1.3 and Zr/V = 0–0.3. The specific activity and yield showed a maximum at Zr/V = 0.1, while the selectivity was maximized over Zr/V = 0.05–0.15. No clear correlation was obtained between catalytic performance and structure.

Takita *et al.* (*6*) examined the role of zinc in VPO catalysts prepared via the aqueous route (Zn/V = 0.11, 0.25). They showed that most of the Zn was present on the surface of the catalyst precursor as a water-soluble compound. The use of Zn/V = 0.11 resulted in a doubling of the conversion and a slight drop in the selectivity (vis-à-vis the unpromoted catalyst). The use of Zn/V = 0.25 gave a similar conversion to the unpromoted catalyst but with a lower selectivity than both Zn/V = 0 (i.e., unpromoted) and Zn/V = 0.11. These authors reported the rate of catalyst oxidation (measured as mass increase in air at 500–600°C) to increase by about 100 times by use of Zn/V = 0.11 (vs Zn/V = 0). They attributed the increased conversion and yield (and lower selectivity) of the catalyst with Zn/V = 0.11 to this increased catalyst oxidation rate. Bej and Rao (*7*) reported the use of a VPO catalyst (P/V = 1.08) containing molybdenum and cerium (Mo/V = 0.03 and Ce/V = 0.007). The promoted catalyst produced higher yields than the unpromoted catalyst but only at higher temperatures. They proposed that Mo increases the selectivity by preventing the reduction of V^{IV} and thus decreasing CO_x formation.

In the present study, we have focused on the use of zirconium as a promoter element in VPO catalysts. The choice of Zr as the promoter element was based on several criteria. First, ZrO_2, when suitably doped, is reported to possess a significant oxygen ion conductivity (*8*). Since the participation of catalytic oxygen in the VPO-catalyzed oxidation of *n*-butane has been indicated in several studies (e.g., *9*, *10*), it was felt that the use of Zr could conceivably enhance/modify the transport of oxygen through the catalyst. Second, $ZrHPO_4$ is reported to be isostructural to the corresponding vanadium compound (*1*). Although the exact nature of the active phase(s) of VPO catalysts is not yet known unequivocally, $(VO)_2P_2O_7$ and various forms of $VOPO_4$ have been cited frequently as important phases. Then the (at least partially) isostructural substitution of Zr for V in the phosphate structure presumably might cause only minimal distortion of the crystal structure. Thirdly, existing reports of Zr as a promoter additive (*5*, *11*) would permit comparison of results from the present study with previous ones in order to establish a clearer picture of the role of Zr.

The objectives of the present study were:

(i) to establish the effects of Zr on the activation and steady-state reaction behavior of VPO catalysts.

(ii) to compare the physicochemical characteristics of an unpromoted VPO catalyst with those of its Zr-promoted counterparts (at "low" and "high" Zr levels, as explained below), and

(iii) to correlate the reaction behavior with the characterization results in order to understand the role of Zr.

METHODS

Catalyst Preparation

The catalysts were prepared via the organic precursor route as discussed by Bremer and Dria (*12*). For the unpromoted catalyst, 9.1 g vanadium pentoxide was dissolved with agitation in a mixture of 130 cm^3 isobutanol and 50 cm^3 allyl alcohol, by heating at 100°C under reflux for 3 h; 11.9 g *ortho*-phosphoric acid was dissolved in 20 cm^3 isobutanol and added to the vanadium solution at 34°C (P/V = 1.2). The solution was then heated at 100–102°C under reflux for 16 h. After it was cooled to 31°C, the bright blue precipitate was separated by filtration, dried in an oven at 150°C for 12 h, ground using a mortar and pestle, and transferred to a dessicator for storage. This

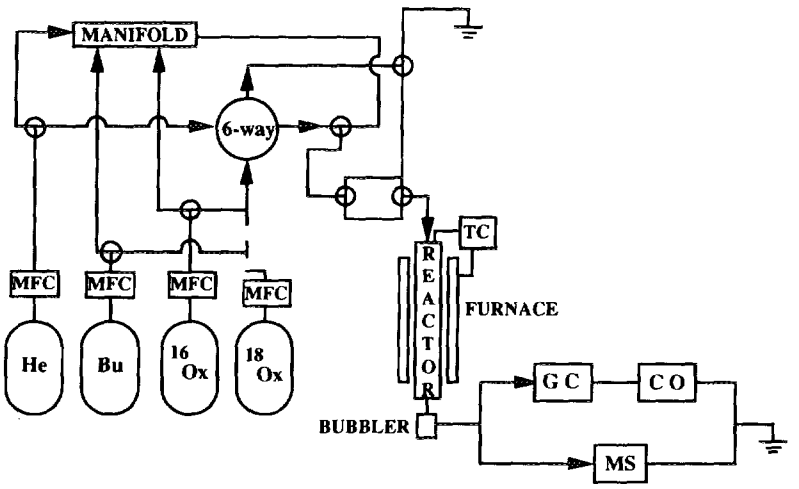

FIG. 1. Schematic of experimental setup: MFC, mass flow controller; TC, temperature controller; GC, gas chromatograph; CO, infrared CO analyzer; and MS, mass spectrometer.

powder is referred to as the VPO catalyst precursor.

Two Zr-containing catalysts were also prepared, with Zr/V = 0.03 and 0.13 (P/V = 1.2, as for the unpromoted catalyst). These are referred to as "low" and "high" levels of Zr, respectively. The preparation method was the same as that described above, except that following the dissolution and partial reduction of V^{5+}, the required mass of zirconium oxide (0.37 and 1.6 g, respectively) was added to the solution at 42–43°C. The suspension was then heated at 100°C under reflux for 1 h, cooled to 34°C, and the solution of *ortho*-H_3PO_4 in isobutanol added as described earlier.

Catalyst Activity Measurements

Catalyst activity measurements were performed in an experimental setup designed for both steady-state and transient experiments. Figure 1 shows a schematic of the experimental setup. Ultrahigh purity helium and CP grade *n*-butane were purified by passage through Alltech oxytraps and dryers to reduce the levels of oxygen and moisture. Ultrahigh purity oxygen was dried before use. The flow rate of each gas was controlled at the desired level by individual Tylan mass flow controllers. A fourth, independent mass flow controller was used to control the flow rate of $^{18}O_2$ (from Isotec, Inc., with a minimum enrichment of 97%) diluted with helium. The setup was designed to permit steady flow as well as step and pulse inputs of single and mixed gases to the reactor. The reactor was a fused silica tube of 12-mm O.D. and 10.3-mm I.D. containing an inner coaxial thermowell of 3-mm O.D. The catalyst powder was placed on a support of glass wool within the reactor which was positioned vertically along the axis of a split-chambered furnace. The reactor temperature was measured by an Omega K-type sheathed thermocouple which along with an Omega model 2010 programmable digital temperature controller was used to control the temperature to within ±0.5°C.

The exit line from the reactor led to a water bubbler where condensates were trapped, followed by a choice of analytical equipment between a Varian 920 gas chromatograph (GC) and a UTI 100C quadrupole mass spectrometer. The GC was equipped with a gas-sampling valve, a 10-foot-long, $\frac{1}{4}$"-diameter Porapak Q column (operated at 111°C), and a thermal conductivity detector. A Spectra-Physics DataJet integrator was

used in conjunction with the GC. Calibration gas mixtures were used to quantify the effluent gas composition. The lines between the reactor and the bubbler, and those between the bubbler and the GC, were heated to 85–90°C to minimize condensation. After passage through the gas-sampling valve, the effluent gases flowed through a Beckman Model 864 infrared carbon monoxide analyzer. The mass spectrometer was equipped to obtain background pressures of 10^{-7} Torr. Gas sampling was achieved through an interface between atmospheric pressure and the 10^{-5}–10^{-7} Torr pressure range (1 Torr = 133.3 Nm^{-2}), while maintaining compositional integrity of the sample.

Catalyst Characterization

Catalyst samples were characterized for bulk structure and surface compositional features by powder X-ray diffraction (XRD) and X-ray photoelectron spectroscopy (XPS). The catalyst samples were characterized after performing the steady-state activity measurements with minimal intermediate exposure to the atmosphere. XRD patterns were obtained on a Diano 8535D automatic X-ray diffractometer. A portion of the catalyst powder was ground further and mounted on a glass slide using rubber cement. XPS spectra were obtained in a Kratos XSAM 800 Auger/ESCA system. For this purpose, another portion of the catalyst powder was pressed into a thin pellet which was mounted on a sample holder using carbon paint.

RESULTS

Catalyst Activation

For each experimental run described below, 0.9 g catalyst precursor was charged to the reactor. The precursor was first calcined in a mixture of flowing oxygen (8 cm^3/min) and helium (30 cm^3/min). The corresponding gas hourly space velocity (GHSV) was about 1775. The following temperature program was used to perform calcination: temperature raised from 25 to 150°C in 10 min, held at 150°C for 1 h, raised from 150 to 400°C over 50 min, held at 400°C for 1 h, and lowered from 400 to 150°C in 1.75 h. This procedure was followed in order to ensure an identical reproducible method for calcining each catalyst.

The general procedure used to activate the catalyst was as follows. The catalyst (i.e., the calcined precursor) was heated to 280°C in flowing helium and oxygen as above. At 280°C, *n*-butane was introduced at 0.75% (by volume of the feed gas mixture). The temperature was then raised to 400°C in stages, and then the analysis of the effluent gas was begun. The system was left for about 20 h with no change in input parameters. Thereafter, the concentration of *n*-butane in the feed was increased in steps to 1.3–1.4%. At each step, a relative steady-state was achieved in about 2 h. After 4 h time-on-stream at 1.4% butane, the system could be shut down and restarted with reproducible performance (i.e., similar conversion and selectivity values prior to shut down and after startup).

Figure 2 shows typical results of the activation procedure for the unpromoted catalyst. Since similar overall trends were also recorded with both promoted catalysts, these latter results are not shown here. Clearly, the *initial* behavior of the catalyst is considerably different from that shown by the *activated* catalyst. The initial high selectivity to maleic (50%) drops rapidly (to about 16%) and then increases slowly to an intermediate value (of about 28%) over the 20-h period at 0.75% butane in the feed. The subsequent increase in the feed butane concentration results in an increased selectivity (to 53%) at fairly constant total conversion. During this stage, the conversion to CO and CO_2 decreases somewhat.

Steady-State
Performance–Temperature Effects

In order to establish the steady-state performance of, as well as any differences among, the three catalysts, each activated catalyst was operated at 1.3–1.4% butane in the feed, and the temperature varied over

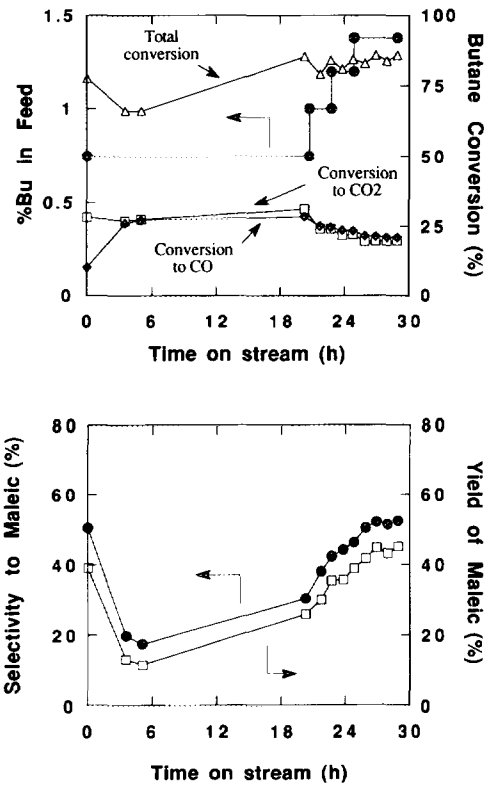

FIG. 2. Activation of unpromoted catalyst. Data at 400°C; GHSV = 1775.

335–440°C. At each new temperature setting, the system was allowed to equilibrate (over a 40-min period) before sample injection. Figure 3 contains results for the effects of temperature on the *total conversion* of butane. Figures 4 and 5 depict the effects of temperature on *selectivity* and *yield* of maleic, respectively. The yield of maleic is calculated as the product of total conversion and selectivity to maleic.

All the catalysts portray the classic selective oxidation rate dependence on temperature, viz., butane conversion increases and maleic selectivity decreases with a rise in temperature. The selectivities, and hence the yields, drop sharply above 400°C. The difference among the catalysts is seen most clearly in Fig. 5. The maximum yield of the high-Zr catalyst is about 43% and occurs

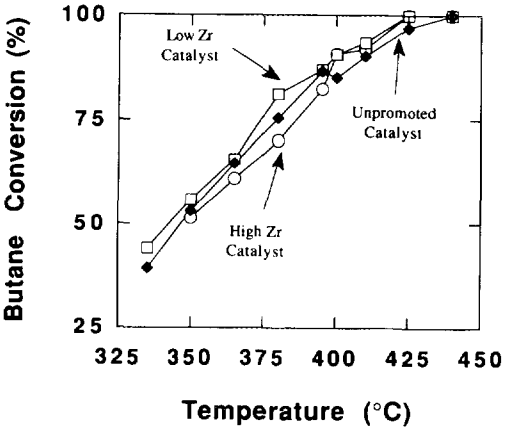

FIG. 3. Effect of temperature on butane conversion: 1.3–1.4% butane in feed; GHSV = 1775; ⊙, high-Zr catalyst; □, low-Zr catalyst; and ◆, unpromoted catalyst.

at 395–400°C. The yield-temperature profile for this catalyst is relatively flat below 400°C. The maximum yields of the unpromoted and the low-Zr catalysts are about 53%. However, this maximum yield occurs at a lower temperature (380°C) for the low-Zr catalyst than for the unpromoted catalyst (395°C). Also, for temperatures below 400°C, the yield–temperature profiles are steeper for these two catalysts than for the high-Zr catalyst.

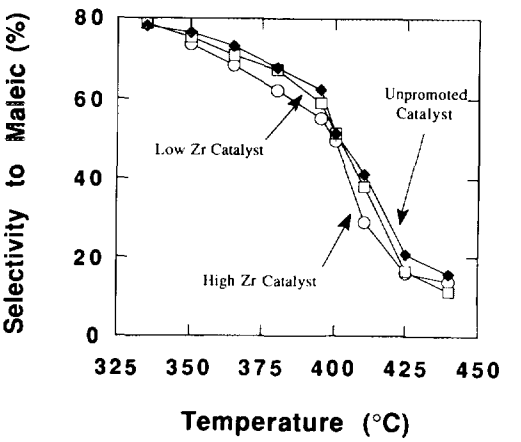

FIG. 4. Effect of temperature on selectivity to maleic: 1.3–1.4% butane in feed; GHSV = 1775; symbols as in Fig. 3.

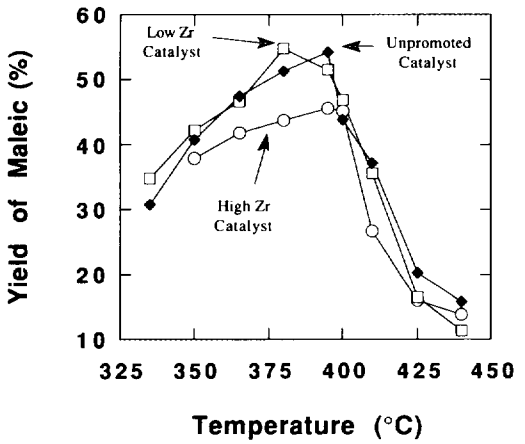

FIG. 5. Effect of temperature on yield of maleic: 1.3–1.4% butane in feed; GHSV = 1775; symbols as in Fig. 3.

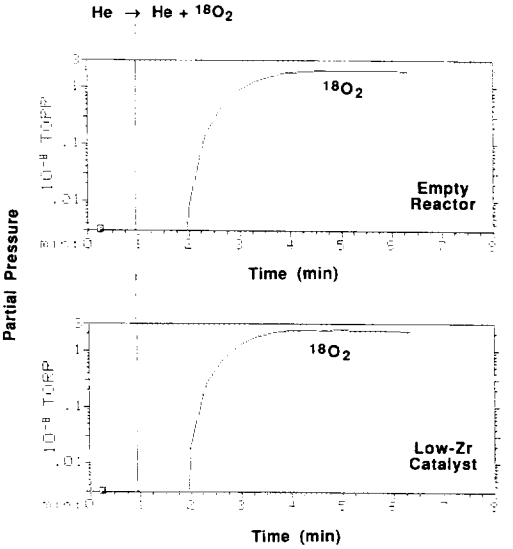

FIG. 6. Response of $^{18}O_2$ in effluent during switch from He to $^{18}O_2$ + He at 400°C.

Oxygen-Exchange Measurements

Experiments were performed in order to evaluate the oxygen-exchange capacity of the catalysts at 400°C using $^{18}O_2$ (*13*). Here, the objective was (a) to exchange ^{16}O in the bulk catalyst lattice with ^{18}O from the gas phase at 400°C, and then (b) to expel any ^{18}O incorporated in step (a) by heating the "exchanged" catalyst from 35 to 515°C in the presence of ^{16}O in the gas phase. For each experiment, about 0.025 g of activated catalyst was charged to the reactor and degassed in flowing helium at 500°C for 30 min. The temperature was then lowered to 400°C and after pausing for 30 min the feed gas stream was switched from helium to a mixture of $^{18}O_2$ and helium (about 20% $^{18}O_2$ by volume). During the entire experiment, the reactor effluent was analyzed continuously using the mass spectrometer. The temperature was held at 400°C until the response for $^{18}O_2$ attained a constant value (Fig. 6). Then the reactor was rapidly cooled to 35°C, and then the feed gas stream was switched from $^{18}O_2$ in helium to $^{16}O_2$ in helium. Thereafter, the reactor was heated from 35 to 515°C at 14°C/min. The experiment was performed with each catalyst and also without any catalyst (i.e., with only glass wool in the reactor). Results are shown in Figs. 6 and 7 for each stage of the experiment, viz., the response of $^{18}O_2$ during the switch at 400°C (Fig. 6), and the response of $^{18}O_2$ and $^{16}O^{18}O$ during the temperature ramp-up from 35 to

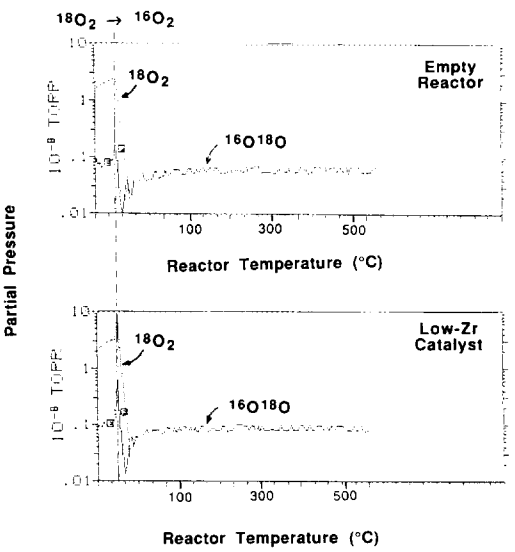

FIG. 7. Response of $^{18}O_2$ and $^{16}O^{18}O$ during switch from $^{18}O_2$ + He to $^{16}O_2$ + He at 35°C, and during subsequent temperature ramp-up from 35 to 515°C.

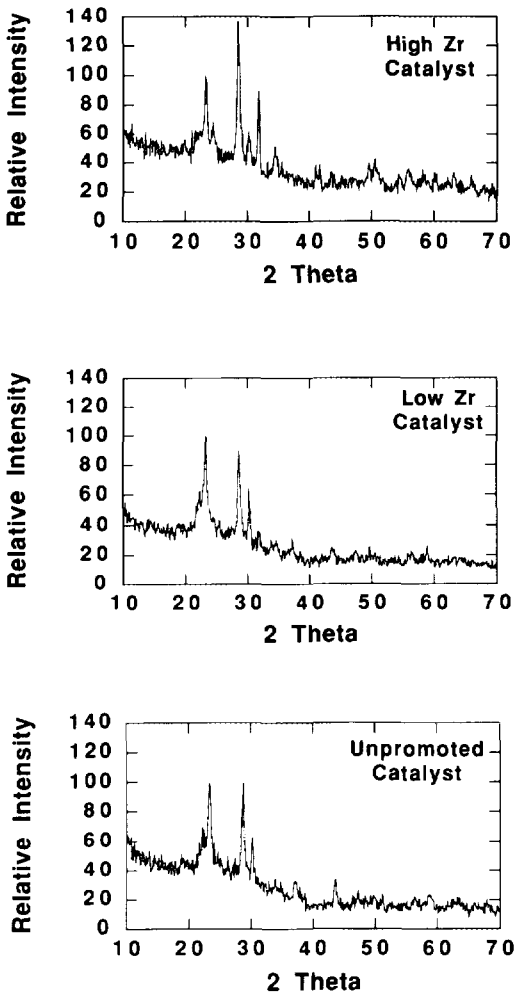

FIG. 8. X-ray diffraction patterns of unpromoted and low- and high-Zr-promoted catalysts.

515°C (Fig. 7). The same response was obtained with the empty reactor as with each catalyst, and no significant exchange of oxygen could be detected between the gas phase and the bulk lattice of the catalyst at 400°C.

X-Ray Diffraction Studies

The XRD patterns of the catalyst samples are shown in Fig. 8. Data on the intensities of major peaks and the corresponding d-spacings are summarized in Table 1. For purposes of comparison, Table 1 also contains relevant data from two other VPO catalyst studies (*9*, *14*). All the samples under study contain the so-called active phase represented by the intense reflections at 3.83–3.86 Å (1Å = 10^{-10} m) and 3.12–3.14 Å, reported to be due to $(VO)_2P_2O_7$ (*15*).

The unpromoted catalyst clearly has a very similar XRD pattern to those of Pepera *et al.* (*9*) and Udovich and Bertolacini (*14*), the latter two also representing unpromoted catalysts. The overall XRD characteristics of the low-Zr catalyst are similar to those of the unpromoted sample. The only significant difference lies in the presence of a low-intensity peak at 2.83 Å in the low-Zr sample. This peak is absent from the unpromoted sample.

The 2.83 Å peak is present in the high-Zr catalyst at a greater intensity than in the low-Zr sample. Additionally, (a) the 3.14-Å peak has a greater intensity in the high-Zr sample than in the other two samples, and (b) the 2.43-Å peak (present at low intensity in the unpromoted and low-Zr samples) is absent from the high-Zr sample.

X-Ray Photoelectron Spectroscopy Studies

The XPS binding energy (B.E.) values have been corrected assuming the C(1*s*) peak to have a B.E. of 284.6 eV. As shown in Table 2, the O(1*s*), V(2*p*), P(2*s*), and P(2*p*) binding energies for both Zr-promoted samples are shifted to lower values relative to the unpromoted sample. The magnitude of the shift varies for the different elements, and is slightly higher for the low-Zr sample. Overall, the B.E. shifts do not appear to be significantly large.

Using the peak areas of P(2*p*) and V(2*p*), and employing the relevant elemental sensitivity factors (0.39 for P(2*p*) and 1.80 for V(2*p*)), the $(P/V)_{surface}$ values vary over the range 2.9–3.3. The results are summarized in Table 3. The presence of Zr does not change $(P/V)_{surface}$ to any significant extent. However, all the $(P/V)_{surface}$ values are significantly greater than the value P/V = 1.2 used in the precursor compounds for catalyst preparation.

TABLE 1

X-Ray Diffraction Patterns of Unpromoted and Zr-Promoted Catalysts

Unpromoted			Low-Zr-promoted		High-Zr-promoted		Pepera *et al.* (*9*)		Udovich and Bertolacini (*14*)	
d-spacing (Å)	2θ (°)	Intens. (%)	*d*-spacing (Å)	Intens. (%)	*d*-spacing (Å)	Intens. (%)	*d*-spacing (Å)	Intens. (%)	*d*-spacing (Å)	Intens. (%)
3.83	23.2	100	3.83	100	3.86	100	3.90	100	3.9	100
3.66	24.3	—	—	—	3.66	68	—	—	—	—
3.12	28.6	100	3.12	90	3.14	137	3.15	98	3.1	58
2.96	30.2	64	2.96	64	2.97	63	2.99	47	3.0	29
2.83	31.6	—	2.83	37	2.83	89	—	—	—	—
2.65	33.9	35	2.60	30	2.61	52	2.67	14	2.7	7
2.43	37.1	33	2.43	31	—	—	2.45	12	—	—
2.08	43.6	34	2.08	26	2.08	34	—	—	—	—
1.57	58.7	24	1.57	27	1.59	37	—	—	—	—

The peak for Zr(3*d*) at 182–185 eV was indistinguishable from the background spectrum for the low-Zr sample. For this sample, Zr/V = 0.03 was used in the precursor compounds. In contrast, the spectrum for the high-Zr sample indicated a broad peak of low intensity at about 182 eV. Comparison of the intensity of this peak with that of V(2*p*), and utilizing the elemental sensitivity factors 1.80 for V(2*p*) and 2.10 for Zr(3*d*), yielded $(Zr/V)_{surface} = 0.03$. This is substantially lower than the value Zr/V = 0.13 used in the precursor compounds for this high-Zr catalyst.

DISCUSSION

The focus of the present study has been on the *promotional effects of zirconium* on the VPO-catalyzed oxidation of *n*-butane and we have therefore utilized information available in the literature on *un*promoted VPO catalysis to the maximum extent possible. Thus, for example, it has not been our intention to study (or optimize) catalyst preparation methods, P/V ratios, or the effects of process parameters such as space velocity on catalyst performance. Given the criteria for the choice of zirconium as the promoter (see the Introduction), Hutchings' review (*1*) was used to select the P/V and Zr/V ratios. Hutchings has attempted to distinguish between two categories of promoted catalysts: (a) Type 1, with P/V > 1 and excess P/promoter ~1, and (b) Type 2, with low promoter/V ratios. Thus our high-Zr catalyst, with P/V = 1.2 and Zr/V =

TABLE 2

XPS Binding Energies

Peak	B.E. (eV) [as is]			B.E. (eV) [corrected for C (1*s*) = 284.6 eV]			B.E. shift (eV) [rel. to sample 1]		
	Sample: 1	2	3	1	2	3	1	2	3
	Zr/V: 0.0	0.03	0.13	0.0	0.03	0.13	0.0	0.03	0.13
C(1*s*)	286.8	288.4	287.4	284.6	284.6	284.6	—	—	—
O(1*s*)	533.2	533.7	532.9	531.0	529.9	530.1	—	−1.1	−0.9
V(2*p*)	518.9	519.6	518.8	516.7	515.8	516.0	—	−0.9	−0.7
P(2*s*)	193.3	193.9	193.4	191.1	190.1	190.6	—	−1.0	−0.5
P(2*p*)	136.2	136.8	136.4	134.0	133.0	133.6	—	−1.0	−0.4

TABLE 3

P/V Ratios

Sample	Zr/V	Peak intensity		Peak width[a]		Peak area		P/V (Uncorrected)		P/V (Corrected)[b]	
		P(2*p*)	V(2*p*)	P(2*p*)	V(2*p*)	P(2*p*)	V(2*p*)	Intens. ratio	Area ratio	Intens. ratio	Area ratio
1	0.00	313.04	464.84	2.54	2.76	795.12	1282.49	0.67	0.62	3.09	2.86
2	0.03	266.34	329.67	3.03	3.39	808.87	1117.91	0.81	0.72	3.74	3.32
3	0.13	303.26	435.16	2.77	2.93	840.33	1275.45	0.70	0.66	3.23	3.05

[a] Peak width at half maximum.
[b] Corrected for sensitivity factors 1.80 (V (2*p*)) and 0.39 (P (2*p*)).

0.13, corresponds to Type 1, while our low-Zr catalyst, with Zr/V = 0.03, corresponds to the Type 2 category.

The results of the activation procedure indicate the critical nature of VPO catalyst activation (Fig. 2). The fairly constant conversion of butane to CO and CO_2 when the total butane conversion increases (at 0.75% butane in the feed) illustrates the evolution of the catalyst towards higher selectivity. This is probably accompanied by a change in the near-surface crystal structure. The subsequent large increase in selectivity, observed when the feed butane concentration is raised from 0.75 to 1.35%, conceivably could be linked to a decrease in the oxidation state of vanadium. For clarity, Fig. 9 shows the dependence of conversion, selectivity and yield on feed butane concentration for all three catalysts. This is in marked contrast to the results of Bej and Rao (*7*) who observed, for both unpromoted and promoted catalysts, that increasing the feed butane concentration resulted in increased conversion and decreased selectivity. No significant difference in operating conditions is apparent, and the dissimilarity in trends is presumably related to the extent of activation. It is significant that our activation process covered a time period of 20–25 h, whereas Bej and Rao (*7*) reported reaching steady state in about 2 h. Centi *et al.* (*2*), on the other hand, have pointed out the long duration (around 200 h) required in order to obtain an equilibrated catalyst. This further underscores the critical nature of the activation process.

The temperature-dependence of conversion, selectivity and yield (Figs. 3–5) clearly shows that, in terms of these performance indices, the high-Zr catalyst is somewhat less active and less selective than the low-Zr and unpromoted catalysts. This is not unexpected since ZrO_2 is known to be a combustion catalyst. There may well be other performance indices, such as catalyst stability or lifetime, for which the high-Zr catalyst could be superior.

The difference between the unpromoted and low-Zr catalysts is less pronounced. Although both exhibit similar maximum yields, the low-Zr catalyst does so at a *lower* temperature. This difference in behavior could arise from various factors. One factor could be a higher surface area for the low Zr catalyst than for the unsupported catalyst. In this case, the low-Zr catalyst would exhibit a higher conversion at a given selectivity (below about 400°C) resulting in yield maximization at a lower temperature. The presence of very low Zr levels then might result in higher surface area catalysts. The available data are not sufficient to substantiate this conclusion. Also, data in the literature indicate that the surface area does not always correlate with catalyst performance. Moreover, one could then expect the higher Zr catalyst to exhibit a higher activity than the other two catalysts, albeit with a lower selectivity. Clearly, this is not the case. Another factor could be that the "low" level of Zr alters the oxygen-transport rates just sufficiently to result in high yields of maleic at reduced temperatures.

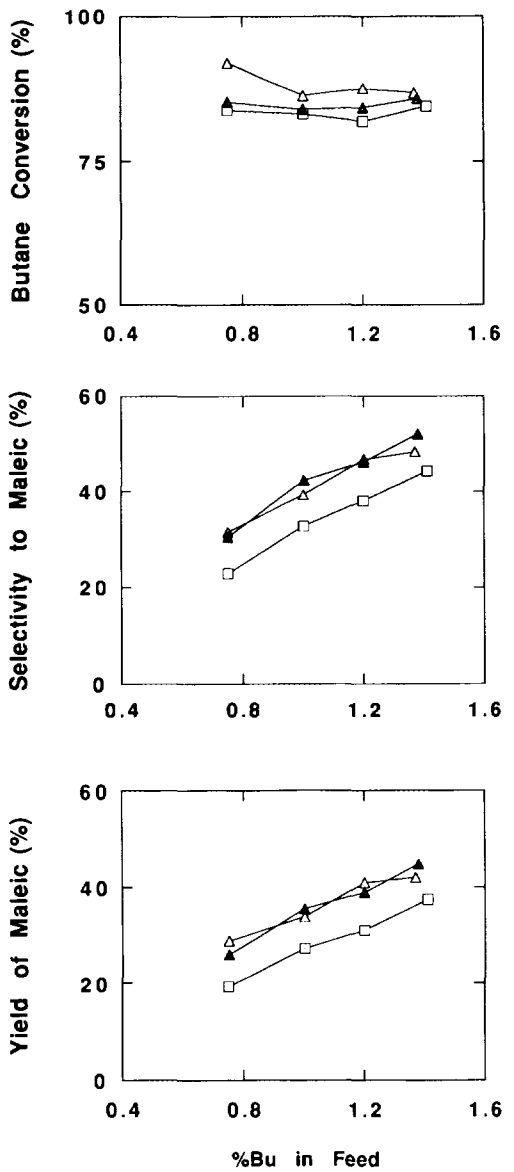

FIG. 9. Effect of feed butane content on butane conversion, and maleic selectivity and yield for (▲) unpromoted and (△) low- and (□) high-Zr-promoted catalysts.

In contrast to our findings, Ai (*5*) reported a maximum maleic yield at Zr/V = 0.1. Several factors may contribute to this difference. Hodnett and Delmon (*3*) cited a study reporting that the promotional effects of Zr were observed only when the Zr precursor was added *before* the phosphorus source. While our method involved addition of Zr *before* P, Ai (*5*) added Zr *after* and *with* the phosphorus. Another significant difference lies in the Zr source, and the resulting physical picture of the catalyst. Our method utilized ZrO_2, wherein Zr would not be incorporated via dissolution. Rather, it would probably involve a physical deposition of some of the VPO precipitate onto ZrO_2 species (XPS and XRD data support this picture, as we discuss later). Ai (*5*) utilized $ZrOCl_2$ which would tend to be more reactive in solution, but since the VPO precipitate was formed *before* the Zr-containing species, the Zr species would be deposited onto the VPO precipitate. Finally, our results (i.e., different optimum temperatures for low-Zr and unpromoted catalysts) point out the importance of studying the performance over a wide temperature range rather than optimizing the promoter/V ratio at a single temperature only.

The $^{16}O_2$–$^{18}O_2$ switching experiments indicate that no significant bulk lattice-gas phase oxygen exchange occurs at 400°C. This is in agreement with the findings of Pepera *et al.* (*9*) that the exchange of surface oxygen is rapid whereas that of bulk oxygen is far slower (a time-frame of hours). The absence of evidence for bulk oxygen exchange persists in the presence of Zr. As we discuss below, the initial indication from our structural characterization points to zirconium being incorporated into the bulk rather than near the surface. Hence, the effects of Zr on the oxygen transport capacity, if any, are probably of a rather small magnitude. However, a beneficial effect of Zr incorporation might require only a small change in oxygen-transport rates. Also, this is in keeping with the rather small magnitude of effects resulting from the incorporation of zirconium.

The similarity between the XRD patterns of our unpromoted catalyst and those of Pepera *et al.* (*9*) and Udovich and Bertolacini (*14*) has been noted previously. The Zr-containing catalysts exhibit a peak at 2.83 Å *d*-spacing. The increase in the intensity of this peak with increasing Zr content, cou-

pled with its absence from the unpromoted catalyst, is taken to signify the presence of a zirconium-containing species. Clearfield and Stynes (*16*) reported *d*-spacings for crystalline zirconium phosphate with a major reflection at 2.64 Å. Additional indications for the preferential presence of zirconium in the bulk (rather than on the surface) are obtained from the XPS studies.

The XPS results in Table 3 indicate a substantially higher value of P/V on the surface (2.9–3.3) than would be expected for the bulk (1.2). This trend is similar to the results of Garbassi *et al.* (*17*), who reported surface P/V values in the range 2.8–2.9 for catalysts with P/V > 1.1 in the bulk. Similarly, Cornaglia *et al.* (*18*) measured surface P/V values of 2.6–3.0 for bulk P/V values above 1.1. Therefore, regardless of the presence of zirconium, VPO catalysts tend to exhibit surface enrichment of phosphorus for bulk P/V values higher than about 1.1. Okuhura *et al.* (*19*), on the other hand, reported surface P/V values which were close to the bulk P/V value of about 1.1. Preliminary findings from deconvolution of the P(2*p*) and V(2*p*) peaks show that the P(2*p*) peak requires (at least) three Gaussian component peaks for a reasonable match. The V(2*p*) peak, on the other hand, is well-represented by two Gaussian component peaks, at 515.5 ± 0.3 eV and at 516.8 ± 0.3 eV. These correspond reasonably well to the B.E. values 515.7 and 517.3 eV reported for V^{4+} and V^{5+} (*17*).

Due to the inherently weaker Zr signal, the estimation of surface Zr/V ratios admittedly is accompanied by greater uncertainties than the estimation of surface P/V ratios. However, it is encouraging to note that in both Zr-containing catalysts, the measured values of surface Zr/V (0 and 0.03) are considerably less than the expected bulk Zr/V values (0.03 and 0.13, respectively). This observation, combined with the XRD observations discussed above, tends to indicate that zirconium is incorporated preferentially in the bulk of the catalyst rather than on the surface.

In conclusion, although the effect of zirconium on VPO catalysis in our study is not very dramatic, Zr is clearly effective at a low concentration and detrimental (in the context of yield maximization) at a high concentration. The role of zirconium is probably of a physical or structural nature rather than producing any new/modified sites or altering the selectivity–conversion behavior. Our results also confirm the preferential incorporation of Zr in the bulk (as anticipated from the preparation procedure), and indicate the formation of an additional crystalline phase, perhaps containing zirconium. The primary role of zirconium could be either to increase the surface area of the catalyst or to alter the oxygen mobility by a small amount. The high-Zr catalyst provides lower yields but with a concomitantly lesser sensitivity to temperature, i.e., a flatter yield–temperature profile (Fig. 5). This may indicate other potential benefits at high Zr levels, namely, improved catalyst stability or lifetime, despite slightly lower product yield in the short term. In this context, it should be pointed out that the promoted VPO catalyst already has a reasonably high selectivity to maleic (~65%) at high butane conversion (~85%).

ACKNOWLEDGMENTS

The authors gratefully acknowledge the assistance of Mr. J.-P. Lebrat with the XRD measurements and Dr. B. Ladna with the XPS measurements, and helpful discussions with Dr. L. A. Cullo of Aristech Chemical Corporation. This work was supported by the Monsanto Fund, by a grant to the Center for Bioengineering and Pollution Control at the University of Notre Dame.

REFERENCES

1. Hutchings, G. J., *Appl. Catal.* **72,** 1 (1991).
2. Centi, G., Trifiro, F., Ebner, J. R., and Franchetti, V. M., *Chem. Rev.* **88,** 55 (1988).
3. Hodnett, B. K., *Catal. Rev.-Sci. Eng.* **27,** 373 (1985).
4. Hodnett, B. K., and Delmon, B., *Appl. Catal.* **6,** 245 (1983).
5. Ai, M., *Appl. Catal.* **28,** 223 (1986).
6. Takita, Y., Tanada, K., Ichimaru, S., Ishihara, T., Inoue, T., and Arai, H., *J. Catal.* **130,** 347 (1991).
7. Bej, S. K., and Rao, M. S., *Appl. Catal. A: Gen.* **83,** 149 (1992).

8. Gellings, P. J., and Bouwmeester, H. J. M., *Catal. Today* **12,** 1 (1992).
9. Pepera, M. A., Callahan, J. L., Desmond, M. J., Milberger, E. C., Blum, P. R., and Bremer, N. J., *J. Am. Chem. Soc.* **107,** 4883 (1985).
10. Contractor, R. M., Bergna, H. E., Horowitz, H. S., Blackstone, C. M., Malone, B., Torardi, C. C., Griffiths, B., Chowdhry, U., and Sleight, A. W., *Catal. Today* **1,** 49 (1987).
11. Jurewicz, A. T., Chu, C.-C., and Young, L. B., Ger. Offen. 2 433 627 (1975).
12. Bremer, N. J., and Dria, D. E., U.S. Patent 4 315 864 (1982).
13. Kalenik, Z., and Wolf, E. E., *Catal. Lett.* **9,** 441 (1991).
14. Udovich, C. A., and Bertolacini, R. J., U.S. Patent 4 328 126 (1982).
15. Busca, G., Cavani, F., Centi, G. and Trifiro, F., *J. Catal.* **99,** 400 (1986).
16. Clearfield, A., and Stynes, J. A., *J. Inorg. Nucl. Chem.* **26,** 117 (1964).
17. Garbassi, F., Bart, J. C. J., Tassinari, R., Vlaic, G., and Lagarde, P., *J. Catal.* **98,** 317 (1986).
18. Cornaglia, L. M., Caspani, C., and Lombardo, E. A., *Appl. Catal.* **74,** 15 (1991).
19. Okuhura, T., Nakama, T., and Misono, M., *Chem. Lett.* **10,** 1941 (1990).